CLOSED-FORM MODAL ANALYSIS OF FLEXURAL BEAM RESONATORS BALLASTED BY A RIGID MASS

G. Scirè Mammano, D. Castagnetti*, E. Dragoni

Dept. of Engineering Sciences and Methods

University of Modena and Reggio Emilia

Via Amendola 2 - 42122 Reggio Emilia – Italy

e-mail: davide.castagnetti@unimore.it; phone: 0039 0522 522634; fax: 0039 0522 522609.

ABSTRACT

The work deals with the study of free flexural vibrations of constant cross-section elastic beams ballasted by a rigid mass with rotary inertia at any longitudinal position. We analyze five sets of boundary conditions of the beam (fixed-free, fixed-fixed, fixed-pinned, pinned-pinned, and free-free) and hypothesize that the structure is perfectly rigid, where the rigid mass is applied. By employing the Euler-Bernoulli beam theory, a single parametric matrix is obtained, which provides the characteristic equation of motion of the structure. When applied to specific configurations, the proposed analytical model predicts the eigenfrequencies and eigenmodes of the beam as accurately as ad-hoc analytical models available in the literature. The accuracy of the results is also confirmed by comparison with detailed two- and three-dimensional finite element analyses of a test case. By means of a 3D finite element model, the applicability of the rigid mass hypothesis to continuous beams with a composite thickened portion is finally assessed.

Keywords: transverse beam vibration, resonator, rigid mass, rotary inertia, modal analysis, MEMS, energy harvesting, tuning.

1. INTRODUCTION

The study of transverse vibrations of beams has always been of great interest due to the extent of practical applications and pervasiveness of beam-like machine elements. Recently, the design of beam resonators with specific eigenfrequencies has gained particular attention in many technological devices, for example: sensors[1], energy harvesting devices[2-3], micro-electro mechanical systems (MEMS)[4], and vibration damping. The design of these structures requires to fulfil three main constraints: a given set of eigenfrequencies in a specific range, the global deformation of the beam under dynamic excitation, and the dimensions of the structure. The most simple and common solution to achieve these constraints is to introduce a distributed inertial element on the beam resonator in order to lower the eigenfrequencies and increase the bending strain, even by keeping the beam short. In particular, this strategy is fairly adopted in the design of energy harvesting devices[5–7].

Many works in the literature deal with the modal analysis of beam structures carrying a concentrated mass. Laura et al.[8] study cantilever beams with a tip mass. Yoo et al. [9] investigate a cantilever beam with a concentrated mass located at an arbitrary position, while Low et al.[10–15] examine a beam constrained at both ends, with the concentrated mass arbitrarily located. The same problem configuration but with compliant constraints is studied by De Rosa et al. [16,17].

The main limitation of these analytical models is that the mass carried by the beam is described as concentrated. The inaccuracy due to this hypothesis increases as the mass dimensions increase. A more accurate analytical model is developed in[18–21], where a rotary inertia is associated to the concentrated mass. In particular, in [18,19] a cantilever beam is examined while a simply supported beam is investigated in [20,21].

Frequently, the cross-section of the ballast mass is thicker than that of the beam. It comes that, as the length of the ballast mass increases a much stiffer structure is obtained. Two modelling techniques can be adopted to deal with this issue. The first technique describes the system as a beam composed by three portions, each with a specific cross-section. This model, which provides good results but is quite complex, is applied [22] where a Euler-Bernoulli beam theory is adopted, and also in [23] by using a Timoshenko beam model. The second modeling technique assumes the ballast mass as rigid, provided that its bending stiffness is higher than that of the beam. This second approach is chosen by Oguamanam[24] and Rama Bhat et al. [25], which investigate a cantilever beam with a distributed mass on the free end.

The aim of this work is to extend this approach to the modal analysis of elastic beams carrying a ballast mass arbitrarily located and undergoing different sets of boundary conditions. The ballast mass is described as a rigid body with mass and rotary inertia. The analysis of eigenmodes and eigenfrequencies refers to a two-dimensional space, describing the two beam portions through the Euler-Bernoulli formulation. Five sets of boundary conditions for the ends of beam are investigated: fixed-free, fixed-fixed, fixed-pinned, pinned-pinned, and free-free. These five sets of boundary conditions are analysed through a closed-form model involving six parameters, which allow to identify each set of boundary condition. Finally, the analytical model has been implemented in a software, which can be freely downloaded at http://www.machinedesign.re.unimore.it/pubblicazioni_eng.html.

The comparison, both with respect to the literature lumped-parameter models, and with respect to two- and three-dimensional finite element (FE) models, shows an excellent accuracy of the proposed method in the prediction of the eigenfrequencies and eigenmodes. Moreover, also the rigid mass hypothesis is assessed showing that it is applicable in all the configurations of practical interest.

2. MODEL DEVELOPMENT

2.1 Reference configuration

Figure 1a shows a cantilever beam having a length *L*, with a ballast mass. This configuration is assumed as reference for the analytical model development. Even if Figure 1a refers to a cantilever beam, the analytical model is developed according to a general formulation, in order to be applied to the following sets of boundary conditions: fixed-free, fixed-fixed, fixed-pinned, pinned-pinned, free-free. The beam structure in Figure 1a consists of three portions. The first, *OP*, is constituted by a beam with a length *a* and constant cross section. The second, *PQ*, represents a ballast mass *m*, with a length *2b*, and an arbitrary cross section. This ballast mass is characterized by a rotary inertia, J_{Gz} , calculated in its centre of mass *G* with respect to the *z* axis (Figure 1a). The distance between the centre of mass *G* and the centre of elasticity of the cross section of the beam is denoted by *d* (portions *OP* and *QR*). Obviously, in case the portion *PQ* would be a composite structure (an inner beam with a top and bottom distributed mass), the mass *m* and rotary inertia J_{Gz} would be those of the composite structure as a whole. Finally, the third portion, *QR*, is a beam with length *c* and the same cross-section as *OP*.

Since the bending stiffness <*EI*> of the ballast mass *PQ* is usually higher than that of the beam portions *OP* and *QR*, we assume the portion *PQ* as infinitely rigid (Figure 1b). Hence, *PQ* is described as a rigid bar, built-in to the portions *OP* and *QR* in *P* and *Q* respectively. Consequently, *PQ* is described by a concentrated mass *m*, and a rotary inertia J_{Sz} , both applied at *S*, the mid-point of the *PQ* segment (Figure 1b). In particular, the rotary inertia J_{Sz} is obtained through the Huygens-Steiner theorem:

$$J_{Sz} = J_{Gz} + md^2 \tag{1}$$

In order to develop the analytical model, the following dimensionless ratios are introduced:

$$\alpha = \frac{m}{\rho A(a+c)} \tag{2}$$

$$\gamma = \frac{J_{sz}}{\rho A(a+c)^3} \tag{3}$$

$$\delta = \frac{2b}{(a+c)} \tag{4}$$

The parameter α represents the ratio between the ballast mass and the mass of the beam itself, while γ is the ratio between the rotary inertia of the ballast mass and that of the beam. Finally, δ is the ratio between the length of the ballast mass and the length of the beam.

2.2 Dynamic equilibrium

The motion of the beam portions *OP* and *QR* can be studied independently by applying appropriate compatibility conditions, which reproduce the rigid kinematic link between points *P* and *Q*. To this aim, a local abscissa is defined along the length of each beam portion (Figure 1b): ξ-axis on *OP* and η-axis on *QR* with domains $0 \le \xi \le a$ and $0 \le \eta \le c$ respectively. For the beam portion *OP*, we define $v(\xi,t)$ as the transverse displacement (*y* direction) at time *t* of the centre of elasticity at coordinate ξ. Thus, the equation of motion of *OP* can be written as [26]:

$$\rho A \frac{\partial^2 v(\xi,t)}{\partial t^2} + EI \frac{\partial^4 v(\xi,t)}{\partial \xi^4} = 0 \tag{5}$$

where ρ is the density of the beam material, *A* the cross section of the beam, *E* the Young's modulus of the beam material, and *I* the inertia moment about the *z* axis of the cross-section of the beam.

Similarly, for the beam portion *QR* we denote $w(\eta,t)$ as the transverse displacement at time *t* of the elastic centre of the cross section at coordinate η. Therefore, the equation of motion can be written in the following form:

$$\rho A \frac{\partial^2 w(\eta,t)}{\partial t^2} + EI \frac{\partial^4 w(\eta,t)}{\partial \eta^4} = 0 \tag{6}$$

A solution of equations (5) and (6) can be expressed as the product of two functions: one of them is a function of the position (ξ or η) and the other one is a harmonic function of time *t*. Since the two beam portions belong to the same vibrating system, the two harmonic functions must coincide. Thus, the solution of equations (5) and (6) can be conveniently expressed by the following functions for *OP* and *QR* respectively:

$$v(\xi,t) = V(\xi)\sin(\omega_n t) \tag{7}$$

$$w(\eta,t) = W(\eta)\sin(\omega_n t) \tag{8}$$

where *V* and *W* are the amplitudes of the transverse displacement in *OP* and *QR* respectively.

Substitution of equations (7) and (8) into equations (5) and (6) respectively, yields the following ordinary differential equations:

$$V^{IV}(\xi) - \beta_n^{\,4} V(\xi) = 0 \tag{9}$$

$$W^{IV}(\eta) - \beta_n^{\,4} W(\eta) = 0 \tag{10}$$

where the Roman superscript indicate the differentiation order with respect to the curvilinear abscissa, while the term $\beta_n^{\;4}$ is defined as:

$$\beta_n^{\;4} = \frac{\rho A}{EI}\omega_n^{\;2} \tag{11}$$

A solution of the ordinary differential equations (9) and (10) may be expressed as:

$$V_n\left(\xi\right) = C_{1n}\cos\left(\beta_n\xi\right) + C_{2n}\sin\left(\beta_n\xi\right) + C_{3n}\cosh\left(\beta_n\xi\right) + C_{4n}\sinh\left(\beta_n\xi\right) \tag{12}$$

$$W_n\left(\eta\right) = D_{1n}\cos\left(\beta_n\eta\right) + D_{2n}\sin\left(\beta_n\eta\right) + D_{3n}\cosh\left(\beta_n\eta\right) + D_{4n}\sinh\left(\beta_n\eta\right) \tag{13}$$

2.3 Boundary conditions

The C_{in} and D_{in} coefficients (eight in total) in equations (12) and (13) respectively, together with the β_n coefficient have to be determined from the boundary conditions at the ends of each beam portion *OP* and *QR* respectively. In particular, four boundary conditions apply to the ends of each beam portion. These boundary conditions involve the displacement functions $V_n(\xi)$ (12) and $W_n(\eta)$ (13) and their derivatives up to the third order. Repeated differentiations of equations (12) and (13) give the following equations:

$$V_n^{\;I}\left(\xi\right) = -C_{1n}\beta_n\sin\left(\beta_n\xi\right) + C_{2n}\beta_n\cos\left(\beta_n\xi\right) + C_{3n}\beta_n\sinh\left(\beta_n\xi\right) + C_{4n}\beta_n\cosh\left(\beta_n\xi\right) \tag{14}$$

$$V_n^{\;II}\left(\xi\right) = -C_{1n}\beta_n^{\;2}\cos\left(\beta_n\xi\right) - C_{2n}\beta_n^{\;2}\sin\left(\beta_n\xi\right) + C_{3n}\beta_n^{\;2}\cosh\left(\beta_n\xi\right) + C_{4n}\beta_n^{\;2}\sinh\left(\beta_n\xi\right) \tag{15}$$

$$V_n^{\;III}\left(\xi\right) = C_{1n}\beta_n^{\;3}\sin\left(\beta_n\xi\right) - C_{2n}\beta_n^{\;3}\cos\left(\beta_n\xi\right) + C_{3n}\beta_n^{\;3}\sinh\left(\beta_n\xi\right) + C_{4n}\beta_n^{\;3}\cosh\left(\beta_n\xi\right) \tag{16}$$

$$W_n^{I}(\eta) = -D_{1n}\beta_n \sin(\beta_n\eta) + D_{2n}\beta_n \cos(\beta_n\eta) + D_{3n}\beta_n \sinh(\beta_n\eta) + D_{4n}\beta_n \cosh(\beta_n\eta) \quad (17)$$

$$W_n^{II}(\eta) = -D_{1n}\beta_n^{2} \cos(\beta_n\eta) - D_{2n}\beta_n^{2} \sin(\beta_n\eta) + D_{3n}\beta_n^{2} \cosh(\beta_n\eta) + D_{4n}\beta_n^{2} \sinh(\beta_n\eta) \quad (18)$$

$$W_n^{III}(\eta) = D_{1n}\beta_n^{3} \sin(\beta_n\eta) - D_{2n}\beta_n^{3} \cos(\beta_n\eta) + D_{3n}\beta_n^{3} \sinh(\beta_n\eta) + D_{4n}\beta_n^{3} \cosh(\beta_n\eta) \quad (19)$$

From Table 1, which collects the five sets of boundary conditions here examined, it appears that only four among the equations (12)-(19) are used to completely define each set of boundary conditions. Although different equations are used for each set of boundary conditions, it is possible to define the following system of four parametric expressions (involving C_{in} and D_{in} coefficients), which conveniently summarize all of them:

$$\begin{aligned}
&\chi_1 C_{1n} + C_{3n} = 0 \\
&-\chi_2 C_{1n} + (\chi_1 - \chi_2) C_{2n} + \chi_2 C_{3n} + (1-\chi_2) C_{4n} = 0 \\
&\chi_3 \cos(\beta_n c) D_{1n} + \chi_3 \sin(\beta_n c) D_{2n} + \cosh(\beta_n c) D_{3n} + \sinh(\beta_n c) D_{4n} = 0 \\
&-\frac{\chi_3 \sin(\beta_n c)}{\chi_5} D_{1n} + \chi_3\,\chi_4\,\chi_5 \cos(\beta_n c) D_{2n} + \frac{\sinh(\beta_n c)}{\chi_6} D_{3n} + \chi_6 \cosh(\beta_n c) D_{4n} = 0
\end{aligned} \quad (20)$$

By substituting the values collected in Table 2 to the six parameters χ_1 , χ_2 , χ_3 , χ_4 , χ_5 , χ_6 , the specific four equations are obtained for each of the five sets of boundary conditions here considered.

The remaining four parameters of equations (12) and (13) can be determined from the compatibility conditions between the beam portions *OP* and *QR* through the rigid link *PQ*. The rigid link *PQ* provides two compatibility conditions, the first dealing with the displacement, the second with the rotation of each beam portions at points *P* and *Q*. The first condition correlates the transverse displacement of points *P* and *Q*, which can be conveniently written as:

$$W_n(Q) = V_n(P) + \delta(a+c) V_n^{I}(P) \tag{21}$$

The second condition equals the rotation of the cross-sections of the beam portions at points *P* and *Q*, yielding the following equation:

$$V_n^{I}(P) = W_n^{I}(Q) \tag{22}$$

The remaining two equations are obtained by imposing the static equilibrium of the rigid link *PQ* (Figure 1b): first, the equilibrium of forces along the transverse *y* direction; second, the equilibrium of moments about the *z*-axis. The first condition deals with shear force *T*, which varies discontinuously between points *P* and *Q* due to the inertial force, F_{im} , of the concentrated mass *m* (at point *S*) and can be written as:

$$T_n(P) - T_n(Q) = -F_{im} \tag{23}$$

where the inertial force F_{im} is defined as:

$$F_{im} = m\omega_n^{2} \sin(\omega_n t)\left[V_n(P) + V_n^{I}(P) b\right] \tag{24}$$

Moreover, the bending moment *M* and shear force *T* for the beam portions *OP* and *QR* satisfy the following expressions:

$$M_n(\xi, t) = EI\, V_n^{II}(\xi) \sin(\omega_n t) \tag{25}$$

$$T_n(\xi,t) = EI\,V_n^{III}(\xi)\sin(\omega_n t) \tag{26}$$

$$M_n(\eta,t) = EI\,W_n^{II}(\eta)\sin(\omega_n t) \tag{27}$$

$$T_n(\eta,t) = EI\,W_n^{III}(\eta)\sin(\omega_n t) \tag{28}$$

By extracting the term ω_n^2 from equation (11) and taking advantage of equations (2) and (4), after little rearrangement which involves equations (23), (24), (26) and (28) we obtain:

$$\left[V_n^{III}(P) - W_n^{III}(Q)\right] + \alpha(a+c)\beta_n^4\left[V_n(P) + (\delta/2)(a+c)V_n^I(P)\right] = 0 \tag{29}$$

With regard to the second static condition, the discontinuity of moments is due to three different contributions: the bending moment originated by the shear force $T_n(Q)$, the bending moment generated by the inertia force F_{im} (equation (24)) of the concentrated mass, and the inertia moment M_{jm} due to the rotation of the rigid link *PQ*. Hence, the following expression is obtained:

$$M_n(P) - M_n(Q) = F_{im}(S)b - T_n(Q)2b + M_{jm} \tag{30}$$

where the inertia moment M_{jm} is defined as:

$$M_{jm} = J_{Sz}V_n^I(P)\omega_n^2\sin(\omega_n t) \tag{31}$$

Finally, by extracting the term ω_n^2 from equation (11) and taking advantage of equations (2)-(4), after some algebraic manipulations which involve equations (24), (25), (27), (28), (30), (31), we obtain:

$$\begin{aligned}&\left[V_n^{II}\left(P\right)-W_n^{II}\left(Q\right)+W_n^{III}\left(Q\right)\delta\left(a+c\right)\right]+\\&-\beta^4\left\{\alpha\left(a+c\right)^2\left(\delta/2\right)\left[V_n\left(P\right)+V_n^{I}\left(P\right)\left(\delta/2\right)\left(a+c\right)\right]+\gamma\left(a+c\right)^3V_n^{I}\left(P\right)\right\}=0\end{aligned} \tag{32}$$

2.4 General solution

The eight boundary and equilibrium conditions (20), (21), (22), (29) and (32) provide the following linear algebraic system in the eight unknowns C_{in} e D_{in}:

$$\mathbf{H}\times\left[C_{1n},\ \ldots,\ D_{4n}\right]^{\mathrm{T}}=\mathbf{0} \tag{33}$$

where the square matrix $\mathbf{H}$ collects the coefficients of the set of equation:

$$\mathbf{H} = \left[\begin{array}{cc}
\multicolumn{2}{l}{\textit{Columns 1 through 2}} \\
\chi_1 & 0 \\
-\chi_2 & \chi_1 - \chi_2 \\
-\cos(\beta_n a) + (a+c)\beta_n \delta \sin(\beta_n a) & -(a+c)\beta_n \delta \cos(\beta_n a) - \sin(\beta_n a) \\
\sin(\beta_n a) & -\cos(\beta_n a) \\
(a+c)\alpha\beta_n \cos(\beta_n a) + \sin(\beta_n a) & (a+c)\alpha\beta_n \sin(\beta_n a) - \cos(\beta_n a) \\
(a+c)^3 \alpha\beta_n^3 \delta^2 \sin(\beta_n a) - 2\left[2 + (a+c)^2 \alpha\beta_n^2 \delta\right]\cos(\beta_n a) & -4\sin(\beta_n a) - (a+c)^2 \alpha\beta_n^2 \delta\left[(a+c)\beta_n \delta \cos(\beta_n a) + 2\sin(\beta_n a)\right] \\
0 & 0 \\
0 & 0
\end{array}\right.$$

$$\begin{array}{cc}
\multicolumn{2}{l}{\textit{Columns 3 through 4}} \\
1 & 0 \\
\chi_2 & 1 - \chi_2 \\
-\cosh(\beta_n a) - (a+c)\beta_n \delta \sinh(\beta_n a) & -(a+c)\beta_n \delta \cosh(\beta_n a) - \sinh(\beta_n a) \\
-\sinh(\beta_n a) & -\cosh(\beta_n a) \\
(a+c)\alpha\beta_n \cosh(\beta_n a) + \sinh(\beta_n a) & \cosh(\beta_n a) + (a+c)\alpha\beta_n \sinh(\beta_n a) \\
\left[4 - 2(a+c)^2 \alpha\beta_n^2 \delta\right]\cosh(\beta_n a) - (a+c)^3 \alpha\beta_n^3 \delta^2 \sinh(\beta_n a) & 4\sinh(\beta_n a) - (a+c)^2 \alpha\beta_n^2 \delta\left[(a+c)\beta_n \delta \cosh(\beta_n a) + 2\sinh(\beta_n a)\right] \\
0 & 0 \\
0 & 0
\end{array} \qquad (34)$$

$$\left.\begin{array}{cccc}
\multicolumn{4}{l}{\textit{Columns 5 through 8}} \\
0 & 0 & 0 & 0 \\
0 & 0 & 0 & 0 \\
1 & 0 & 1 & 0 \\
0 & 1 & 0 & 1 \\
0 & 1 + (1/2)(a+c)^2 \alpha\beta_n^2 \delta & 0 & (1/2)(a+c)^2 \alpha\beta_n^2 \delta - 1 \\
4 & -4\left[(a+c)^3 \beta_n^3 \gamma + (a+c)\beta_n \delta\right] & -4 & 4\left[-(a+c)^3 \beta_n^3 \gamma + (a+c)\beta_n \delta\right] \\
\chi_3 \cos(\beta_n c) & \chi_3 \sin(\beta_n c) & \cosh(\beta_n c) & \sinh(\beta_n c) \\
-\dfrac{\chi_3 \sin(\beta_n c)}{\chi_5} & \chi_3 \chi_4 \chi_5 \cos(\beta_n c) & \dfrac{\sinh(\beta_n c)}{\chi_6} & \chi_6 \cosh(\beta_n c)
\end{array}\right]$$

The linear system (33) has a non trivial solution if and only if the determinant of the $\mathbf{H}$ matrix equals zero:

$$\det(\mathbf{H}) = 0 \qquad (35)$$

Equation (35) is the characteristic transcendental equation of the system that can be solved for the variable β_n, obtaining infinite roots. According to equation (11), each root identifies a circular frequency ω_n of the *n*-th eigenmode of the beam. For each circular frequency ω_n it is possible to determine the C_{in} and D_{in} constants through the set of equation (33). Since the determinant of the characteristic matrix $\mathbf{H}$ is zero, for each circular frequency ω_n the equations of the system are linearly dependent. Therefore, we need to set an arbitrary value for one of the unknown constants and then calculate the remaining ones. Upon substitution in equations (12) and (13) of the parameters C_{in} and D_{in} , the expressions of the eigenmodes associated to each circular frequency ω_n are obtained, up to a multiplicative coefficient.

In conclusion, this method, which will be called from now on Rigid Mass (RM) model, provides the eigenfrequencies and eigenmodes of an elastic beam under generic constraints, carrying a ballast rigid mass. It is observed that, by simply setting the semi-length b of the ballast mass equal to zero, the RM model simplifies to a model that describes the inertial element (m, J_{Sz}) as concentrated. This model, from now on called Concentrated Mass (CM) model, is analogous to the models retrieved in the literature [18–21]. If, in addition, also the rotary inertia J_{Sz} of the ballast mass is set to zero, the CM model describes a concentrated mass without inertial effects [8–17].

3. MODEL VALIDATION

In order to simplify the calculation procedure, the RM model has been implemented in a software (named Beam Frequency Calculator (BFC)), through the commercial tool Visual Basic 6.0. The software can be freely downloaded from the web at [27]. Appendix 1 describes, for a particular configuration, all the details of the software and its application.

In this section the assessment of the model is performed in three steps. The first assessment compares the CM model to analogous model taken from the literature. The second assessment, which is focused on a case study, compares the RM model with a two-dimensional FE model, a three-dimensional FE model, and finally with the literature models. The third assessment deals with the applicability of the rigid mass hypothesis.

3.1 Comparison between the CM model and literature models

In order to assess the correctness of the proposed model, in this section we compare the CM model to analogous models retrieved from the literature (either considering concentrated mass with rotary inertia or a concentrated mass without rotary inertia). The comparison is performed for all the five sets of boundary conditions considered in Section 2. The CM model is solved through the BFC software [27].

Four analytical models taken from the literature are used for comparison. First, the model presented in [15] for the case of a cantilever beam with a tip mass with rotary inertia. Second, the model proposed in [8], which is applied both to the case of a fixed-fixed beam and to the case of a fixed-pinned beam with intermediate concentrated mass without rotary inertia. Third, the model proposed in [17] for a pinned-pinned beam configuration having an intermediate concentrated mass with rotary inertia. Fourth, the model presented in [21] for the case of a free-free beam without any inertial element.

Table 3 compares, for each of the five sets of boundary conditions, the first four normalized eigenfrequencies provided by the literature models with those provided by the CM model.

Specific values of the non-dimensional parameters m/m_{beam} , $J/(m_{beam}*L^2)$, a/L have been considered for each configuration.

3.2 Comparison with respect to a cantilever having an intermediate ballast mass

Figure 2 shows the sketch of a cantilever with an intermediate ballast mass, eccentric with respect to the midplane of the beam. This configuration is taken as reference in this second step of assessment of the RM model. The structure consists of a beam with rectangular cross-section. Two ballast masses of different thickness are attached along the free length of the beam to the upper and bottom face respectively. On the whole, the region containing the ballast masses has a mass m (see Section 2).

The same steel material is assumed (Young's modulus 210 GPa, Poisson's ratio 0.3, and mass density 7850 kg/m^3) both for the beam and for the inertial elements. We examined all the five sets of boundary conditions described in Table 1. In particular, in the case of asymmetric constraints (fixed-free and fixed-pinned) the fixed constraint is applied to the left end of the beam that is the farthest from the ballast mass.

3.2.1 RM model

The configuration in Figure 2 has been studied applying the RM model in its full formulation (ballast mass described as rigid and with finite length). Thus, in accordance with the sketch in Figure 1b, the beam in Figure 2 can be described by the geometric and inertial properties collected in Table 4 (RM model). The analysis has been performed through the BFC software.

Tables 5 and 6 report the first four eigenfrequencies provided by the RM model, and by the two- and three-dimensional FE models (see Section 3.2.2 and Section 3.2.3) respectively, for each set of boundary condition. Moreover, Tables 5 and 6 presents the percentage relative error, which was calculated with respect to the FE model.

Figure 3, 4, 5, 6 and 7 present, in normalized form, the first four eigenmodes provided by the RM model (hollow circles) for the fixed-free, fixed-fixed, fixed-pinned, pinned-pinned and free-

free constraint respectively. The hollow circles are not plotted where the ballast mass occurs, in order to make it clearly visible.

3.2.2 Two-dimensional FE model

The two-dimensional FE model describes the configuration in Figure 2 and was implemented through the commercial FE software ABAQUS V6.9.1 [28]. The two beam portions have been described through linear Euler beam elements (B21H), with full integration. According to a convergence procedure, the element length was set to 0.05 mm, giving a total of 1500 elements.

The rigid mass linking the beam portions was described thorough a kinematic “wire connector”, available in ABAQUS. This is a rigid kinematic link between the ends (*P* and *Q*) of the beam portions, which equals their corresponding kinematic degrees of freedom (Figure 1). A mass m and a rotary inertia J_{Sz} (according to Table 4) are imputed to the midpoint of this kinematic link. The material of the beam is described as linear elastic with the mechanical properties of steel defined in Section 3.2.

Five different models have been implemented, one for each set of boundary conditions in Table 1, giving the results presented in Table 5, which is organized as described in Section 3.2.1.

3.2.3 Three-dimensional FE model

The three-dimensional FE model describes in details the configuration in Figure 2 and is assumed as the reference solution for the modal analysis of this case study. As the previous two-dimensional FE model, it was implemented through the ABAQUS software [28]. The whole structure has been described through eight-noded, linear, hexahedral elements (C3D8R), with reduced integration and hourglass control [28]. According to a convergence analysis, not reported here for the sake of brevity, the element side length was set 0.25 mm, except in the thickness of the beam direction, where six layers of elements with the same transverse side length as above were applied (Figure 8). On the whole, the mesh consists of 320,000 elements, 346,983 nodes and 1,040,949 degrees of freedom. As in the previous two-dimensional FE model, the material was described as linearly elastic, according to the values of Section 3.2. Five different models have been implemented, one for each set of boundary condition described in Table 1.

Table 6 displays, for all the constraint conditions, the results provided by this computational model, organized as described in Section 3.2.1. Figures 3, 4, 5, 6 and 7 show, in normalized form, the first four eigenmodes provided by the computational model (solid line) for the fixed-free, fixed-fixed, fixed-pinned, pinned-pinned and free-free constraint respectively.

3.2.4 Literature models

To the aim of evaluating the accuracy of the literature models in the prediction of the modal response of a beam carrying a ballast mass in arbitrary position, they are applied to the case study in Figure 2. The CM model was used as a substitute of the literature models due to its optimal agreement with the models taken from the literature (see Discussion section), to its easiest implementation, and to the need to investigate many sets of boundary conditions. The values of the geometric and inertial properties used in this comparison are collected in Table 4, for concentrated mass and rotary inertia and concentrated mass without rotary inertia respectively.

Table 6 shows, for all the constraint conditions in Table 1, the results provided by the CM model in both forms (with and without rotary inertia), organized as described in Section 3.2.1. Figures 3, 4, 5, 6 and 7 display, in normalized form, the first four eigenmodes provided by the CM model, with rotary inertia (hollow triangles) and without rotary inertia (crosses), for the fixed-free, fixed-fixed, fixed-pinned, pinned-pinned and free-free constraint respectively.

3.3 Assessment of the rigid mass hypothesis

This last step aims at assessing the applicability of the rigid mass hypothesis (Section 2). Therefore, the analysis evaluates the sensitivity of the analytical model to the ratio between the bending stiffness of the ballast mass cross-section and that of the beam cross-section. Figure 2 highlights that both the beam and the ballast masses contribute to the bending stiffness of the ballast mass cross-section. Hence, it is possible to define the bending stiffness ratio φ as follows:

$$\varphi = \frac{< EI >_{mass}}{< EI >_{beam}} \tag{36}$$

where $< EI >_{mass}$ and $< EI >_{beam}$ are calculated for a generic cross section, which can eventually be inhomogeneous (Appendix 2). The investigation was performed referring to the configuration of Figure 2, for two constraint conditions: fixed-free and fixed-fixed (Table 1).

In order to simplify the procedure, the bending stiffness ratio φ was varied by changing only the value of the Young's modulus of the inertial element E_{mass} , while keeping constant all the other parameters. Since the sensitivity analysis was performed through the three-dimensional FE model presented in Section 3.2.3, the same geometry and mass properties of the structure were used all along. Therefore, where the ballast masses are introduced, the cross-section of the structure comprises three layers with different Young's modulus.

Table 7 summarizes the values adopted for the elastic modulus of the ballast mass and the corresponding values of the bending stiffness ratio φ. Figures 9 and 10 show for the fixed-free and fixed-fixed beam respectively, the percentage relative error of the RM model on the first four eigenmodes, as a function of the bending stiffness ratio φ. The relative error was calculated with respect to the three-dimensional FE model.

4. DISCUSSION

The RM model consists of an algebraic system of eight linear equations in eight unknowns, represented, in matrix notation, by (39). These equations depend on the elastic and geometric properties of the beam and on the inertial properties of the rigid ballast mass. In addition, they include 6 parameters (χ_{i} , i = 1..6), which are a function of the set of boundary conditions of the structure being examined.

By examining the RM model, we observe that by setting to zero some of the model parameters, the model reduces to the classical analytical model presented in the literature[6–11,14,15] that describe the added ballast mass as concentrated. In particular:

- $b = 0$: concentrated ballast mass;
- $J_{sz} = 0$: ballast mass without rotary inertia;
- $m = 0$: ballast mass without mass.

Table 3 shows the excellent accuracy of the CM model when compared to the classical models from the literature, for all the eigenfrequencies and sets of boundary conditions examined. Therefore, the CM model unifies, in a general approach and for several sets of boundary conditions, the literature models.

Table 5 highlights that the results from the RM model and from the two-dimensional FE model closely match. The perfect agreement between the two methods, which testifies the accuracy of the RM model, is imputable to the same underling hypotheses (Euler beam formulation and rigid mass).

Two observations can be made by examining Table 6. First, the RM model provides very accurate results also in comparison with the three-dimensional FE model, with an error ranging from 0.7% to 2%. In particular, the RM model always exceeds the FE model prediction since it assumes a rigid mass and does not account for the shear deformability of the beam. Second, literature models (represented by the CM model) provide an error ranging from 1.6% (at the first eigenfrequency for the fixed-free constraint), up to a maximum of 54% (at the fourth eigenfrequency for the fixed-pinned constraint). In particular, the forecasts of the literature models without rotary inertia either overestimate or underestimate the numerical forecasts. This alternate error is connected to a poor accuracy in the calculation of the eigenmode as can be seen from the diagrams in Figures 3-7. By contrast, the literature models with rotary inertia always underestimate the numerical forecasts, with higher percentage relative errors. This is due to the fact that the underestimation of the stiffness in the region of the ballast mass (PQ). On the whole, in comparison to the literature models (represented by the CM model) the RM model predicts much more accurately the eigenfrequencies of the beam for whichever constraint is considered.

Figures 3-7 highlight the excellent agreement between the RM model (hollow circles) and the three-dimensional FE model (solid line). A little discrepancy between these models occurs only at the fourth eigenfrequency of the fixed-pinned beam (Figure 5). This is imputable to the complex curvature in the transition region between the beam and the ballast mass, which is described by the FE model. In addition, the straight deformed shape of the ballast mass (solid line in Figures 3-7) fully justifies the rigid mass hypothesis for the case study here examined.

Figures 3-7 highlight that the concentrated mass model without rotary inertia (crosses) and the concentrated mass model with rotary inertia (hollow triangles) provide with fair accuracy only the first or second eigenmodes depending on the set of boundary conditions. By contrast, the predictions of the higher eigenmodes, which are fairly complex, are completely wrong. In conclusions, the models that describe the mass as concentrated, artificially alter the stiffness of the structure, thus providing an incorrect mode shape prediction.

From Figures 9 and 10 we can see that for both beam configurations examined, the error of the RM model decreases as the bending stiffness ratio φ increases. Obviously, this can be attributed to the hypothesis of rigid mass underling the RM model. In the case of the fixed-free beam (Figure 9), with exception of the third eigenmode, the error is lower than 11% up to φ

equal to 50. The higher error for the third eigenmode (10% at a bending stiffness ratio equal to 200) is imputable to the significant bending strain occurring in this eigenmode near the rigid mass (solid line in Figure 3). Finally, Figure 9 highlight that the bending stiffness ratio does not affect the accuracy of the first eigenfrequency prediction for this constraint condition.

Figure 10 shows a higher error than in Figure 9 for all the eigenfrequencies at corresponding values of φ. On the whole, however, the error is more uniform between eigenmodes. This, once again, can be attributed to the higher deformation occurring for the eigenmodes in this constraint condition (fixed-fixed), which, consequently, can be less accurately described by the RM model.

On the whole, the hypothesis of a rigid ballast massis fully justified when the bending stiffness ratio is high, as usually occurs in practice. For example, assuming the same material for the beam and ballast massand a ratio between the cross-section in the region of the ballast massand that of the beam equal to 2, 4 or 8, the bending stiffness ratio φ equals 8, 64, and 512 respectively. In the case study in Figure 2, the ratio φ is 3350. When the stiffness ratio is higher than 1000, the error is lower than 3% on the first four eigenfrequencies, thus comparable to a computational model.

In conclusion, the assessment of the RM model testifies its great accuracy for a wide range of beam configurations with ballast mass. The method can be applied to whichever beam section, including inhomogeneous section beam. Since the model relies on the Euler-Bernulli beam theory, its accuracy decreases when thick beams are examined, in particular in the prediction of the higher eigenmodes. Much more details about this can be found in the works from Grant [29] and Han et al. [30].

5. CONCLUSIONS

The paper develops the Rigid Mass (RM) model for the modal analysis of a constant cross-section beam, carrying a ballast mass for resonance tuning. As main hypotheses, the model describes the beam according to the Euler-Bernoulli formulation and the ballast mass as rigid, with mass and rotary inertia. Five sets of boundary conditions can be examined through the RM model, which reduces to a square matrix (dimension eight per eight) that provide the characteristic equation and thus the eigenfrequencies and eigenmodes of the structure. When reduced to describe the ballast mass as a concentrated mass either with or without inertia, the RM model provides results that match closely those of the analogous models from the literature. A very good agreement is obtained also in the comparison between the RM model and the two- and three-dimensional FE models. By contrast, the literature models describing the ballast massas a concentrated mass either with or without rotary inertia, can lead to noticeable errors in the eigenfrequencies and eigenmodes prediction. With regard to the rigid mass hypothesis, the results show that it is a good approximation for the great majority of the resonator structures occurring in practice.

Funding

This research received no specific grant from any funding agency in the public, commercial, or not-for-profit sectors.

REFERENCES

1. Hassanpour P, Cleghorn WL, Mills JK, Esmailzadeh E. Exact solution of the oscillatory behavior under axial force of a beam with a concentrated mass within its interval. *J Vib Control [Internet]*. 2007 Dec 1 [cited 2014 Jul 25];13(12):1723–1739. Available from: http://jvc.sagepub.com/cgi/doi/10.1177/1077546307076285

2. Roundy S, Wright PK. A piezoelectric vibration based generator for wireless electronics. *Smart Mater Struct [Internet]*. 2004 Oct 1 [cited 2014 Jul 10];13(5):1131–1142. Available from: http://stacks.iop.org/0964-1726/13/i=5/a=018?key=crossref.8cb539ef2c04efdc61df2fae9dc8e48c

3. Jinkui C, Haijun Z, Xiaozhen D, Shuanghui W. The electrical characteristic simulation of cantilever beam used in micro battery [Internet]. In: International Technology and Innovation Conference 2006 (ITIC 2006). Iee; 2006. p. 160–165.Available from: http://digital-library.theiet.org/content/conferences/10.1049/cp_20060748

4. Zurn S, Hsieh M, Smith G, Markus D, Zang M, Hughes G, et al. Fabrication and structural characterization of a resonant frequency PZT microcantilever. *Smart Mater Struct [Internet]*. 2001 Apr 1;10(2):252–263. Available from: http://stacks.iop.org/0964-1726/10/i=2/a=310?key=crossref.77b569f3c5cff167917bbfdff0103998

5. Brusa E, Bona F De, Gugliotta A, Somir A. Dynamics modeling of microbeams under electrostatic load. In: DTIP2003 of MEMS & MOEMS. 2003. p. 5–7.

6. De Marqui Junior C, Erturk A, Inman DJ. An electromechanical finite element model for piezoelectric energy harvester plates. *J Sound Vib [Internet]*. 2009 Oct [cited 2014 Jul 24];327(1-2):9–25. Available from: http://linkinghub.elsevier.com/retrieve/pii/S0022460X09004520

7. Ferrari M, Ferrari V, Guizzetti M, Marioli D, Taroni A. Piezoelectric multifrequency energy converter for power harvesting in autonomous microsystems. *Sensors Actuators A Phys [Internet]*. 2008 Mar [cited 2014 Jul 9];142(1):329–335. Available from: http://linkinghub.elsevier.com/retrieve/pii/S0924424707005481

8. Laura PAA, Pombo JL, Sushemil EA. A note on the vibrations of a clamped-free beam with a mass at the free end. 1974;37:161–168.

9. Yoo HH, Seo S, Huh K. The effect of a concentrated mass on the modal characteristics of a rotating cantilever beam. 2002;216(July 2001):151–163.

10. Low KH. A note on the fundamental shape function and frequency for beams under off-center load. *J Sound Vib.* 1997;202(1):134–138.

11. Low KH. A comparative study of the eigenvalue solutions for mass-loaded beams under classical boundary conditions. *Int J Mech Sci [Internet]*. 2001 Jan;43(1):237–244. Available from: http://linkinghub.elsevier.com/retrieve/pii/S0020740399001137

12. Low KH. On the eigenfrequencies for mass loaded beams under classical boundary conditions. *J Sound Vib [Internet]*. 1998 Aug [cited 2014 Jul 28];215(2):381–389. Available from: http://www.sciencedirect.com/science/article/pii/S0022460X98916261

13. Low KH. Closed-form formulas for fundamental vibration frequency of beams under off-centre load. *J Sound Vib [Internet]*. 1997 Apr [cited 2014 Jul 28];201(4):528–533. Available from: http://www.sciencedirect.com/science/article/pii/S0022460X96907063

14. Chai GB, Low KH. On the natural frequencies of beams carrying a concentrated mass. *J Sound Vib.* 1993;160(1):161–166.

15. Naguleswaran S. Lateral vibration of a uniform euler–bernoulli beam carrying a particle at an intermediate point. *J Sound Vib [Internet]*. 1999 Oct [cited 2014 Jul 28];227(1):205–214. Available from: http://www.sciencedirect.com/science/article/pii/S0022460X99922769

16. De Rosa MA, Ascoli S, Nicastro S. Letter to the editor: exact dynamic analysis of beam-mass systems. *J Sound Vib [Internet]*. 1996 Oct [cited 2014 Jul 28];196(4):529–533. Available from: http://www.sciencedirect.com/science/article/pii/S0022460X96905003

17. De Rosa MA, Franciosi C, Maurizi MJ. On the dynamic behaviour of slender beams with elastic ends carrying a concentrated mass. *Comput Struct.* 1996;58(6):1145–1159.

18. Bruch JC, Mitchell TP. Vibrations of a mass-loaded clamped-free Timoshenko beam. *J Sound Vib [Internet]*. 1987 Apr;114(2):341–345. Available from: http://linkinghub.elsevier.com/retrieve/pii/S0022460X8780158X

19. Swaminadham M, Michael A. A note on frequencies of a beam with a heavy tip mass. *J Sound Vib.* 1979;66(1):144–147.

20. Hamdan MN, Jubran BA. Free and forced vibrations of a restrained uniform beam carrying an intermediate lumped mass and a rotary inertia. *J Sound Vib.* 1991;152(2):203–216.

21. Srinath LS, Das YC. Vibrations of Beams Carrying Mass. *J Appl Mech Trans ASME.* 1967;34(784):785.

22. Naguleswaran S. Vibration of an Euler–Bernoulli beam on elastic end supports and with up to three step changes in cross-section. *Int J Mech Sci [Internet]*. 2002 Dec [cited 2014 Jul 29];44(12):2541–2555. Available from: http://www.sciencedirect.com/science/article/pii/S002074030200190X

23. Ju F, Lee HP, Lee KH. On the free vibration of stepped beams. *Int J Solids Struct.* 1994;31(22):3125–3137.

24. Oguamanam DCD. Free vibration of beams with finite mass rigid tip load and flexural–torsional coupling. *Int J Mech Sci [Internet]*. 2003 Jun [cited 2014 Jul 25];45(6-7):963–979. Available from: http://linkinghub.elsevier.com/retrieve/pii/S0020740303001747

25. Rama Bhat B, Wagner H. Natural frequencies of a uniform cantilever with a tip mass slender in the axial direction. *J Sound Vib.* 1976;45(2):304–307.

26. Kelly SG. Fundamentals of mechanical vibrations. 2nd ed. McGraw-Hill Science; 2000.

27. Machine Design Group Reggio Emilia [Internet]. *2012.* Available from: http://www.machinedesign.re.unimore.it/pubblicazioni_eng.html

28. SIMULIA ABAQUS, User‘s Manual. 2008;

29. Grant DA. The effect of rotary inertia and shear deformation on the frequency and normal mode equations of uniform beams carrying a concentrated mass. *J Sound Vib.* 1978;57(3):357–365.

30. Han SM, Benaroya H, Wei T. Dynamics of transversely vibrating beams. *J Sound Vib.* 1999;225(5):935–988.

31. Gay D, Hoa S V. Composite materials, design and applications. 2nd ed. CRC Press; 2007.

1 Notation

a	Length of the left beam portion (Figure 2)
A	Cross-section area of the beam
A_i	Cross-section area of the *i*-th layer of the inhomogeneous section
b	Half-length of the ballast mass (Figure 2)
c	Length of the right beam portion *QR* (Figure 2)
C_{in}	*i*-th parameter of the *n*-th eigenshape of the beam portion *OP*
D_{in}	*i*-th parameter of the *n*-th eigenshape of the beam portion *QR*
E	Young's modulus of the beam material
Ec	Elastic centre of the inhomogeneous section
E_i	Young's modulus of the material of the *i*-th layer of the inhomogeneous section
E_{mass}	Young's modulus of the ballast mass material
F_{im}	Inertia force in the transverse direction arising from the ballast mass
G	Centre of mass of the ballast mass
h_E	Distance between the centre of elasticity of the inhomogeneous section and the longitudinal axis of the beam
h_i	Thickness of the *i*-th layer of the inhomogeneous section
$\underline{\underline{\boldsymbol{H}}}$	Characteristic matrix of the set of equations of motion

I_z	Inertia moment of the cross-section of the beam about the z-axis
$I_{iz'}$	Inertia moment of the cross-section of the i-th layer of the inhomogeneous section about the z'-axis
J_{Gz}	Inertia moment of the inertial element m, calculated in the centre of mass, about the z-axis
J_{Sz}	Inertia moment of the inertial element m , calculated in point S (Figure 1b), about the z-axis
L	Total length of the beam
m	Mass of the ballast mass
M_{Jm}	Moment originated by the inertial angular acceleration on the mass m
$M_n(\xi, t)$	Bending moment acting at ξ coordinate and time t of the beam portion OP for the n-th eigenmode
$M_n(\eta, t)$	Bending moment acting at η coordinate and time t of the beam portion QR for the n-th eigenmode
r	Width of the inhomogeneous section beam
$T_n(\xi, t)$	Shear force acting at ξ coordinate and time t of the beam portion OP for the n-th eigenmode
$T_n(\eta, t)$	Shear force acting at η coordinate and time t of the beam portion OP for the n-th eigenmode

t	Time coordinate
$v(\xi, t)$	Transverse displacement of the centre of mass of the beam portion *OP* at ξ coordinate and time t
$V_n(\xi)$	Amplitude of the transverse displacement of the centre of mass of the beam portion *OP* for the n-th eigenmode
$w(\xi, t)$	Transverse displacement of the centre of mass of the beam portion *QR* at ξ coordinate and time t
$W_n(\xi)$	Amplitude of the transverse displacement of the centre of mass of the beam portion *QR* for the n-th eigenmode
y_i	Ordinate of the geometric centre of the i-th layer of a inhomogeneous section
z	Axis normal to the page and directed outward in the *xyz* reference system
α	Ratio between the mass of the ballast mass and the mass of the beam
β_n	n-th root of the transcendental equation
γ	Ratio between the rotary inertia of the ballast mass and that of the beam
δ	Ratio between the length of the ballast mass and the free length of the beam
η	Curvilinear abscissa of the beam portion *QR*
ξ	Curvilinear abscissa of the beam portion *OP*
ρ	Mass density of the beam material

$\bar{\rho}$	Equivalent average mass density of the material constituting the inhomogeneous section
ρ_i	Average mass density of the material of the *i*-th layer of the inhomogeneous section
φ	Bending stiffness ratio between the cross section of the ballast mass and that of the beam
$\chi_{1,\ldots,6}$	Parameters to define the specific set of boundary conditions
ω_n	Circular frequency of the *n*-th eigenmode
$I, II,\ldots,IV$	Derivation order
$<EI>_{beam}$	Bending stiffness of the cross-section of the beam section
$<EI>_{mass}$	Bending stiffness of the cross-section of the ballast mass
$<EI_{iz'}>$	Equivalent bending stiffness of the inhomogeneous cross-section

APPENDIX 1

The model developed in this work (RM model) has been implemented in software through the commercial tool Visual Basic 6.0, and can be freely downloaded from the web [27]. In the following we describe the simple procedure to perform an analysis.

From the main window of the software, click on the START button (or on File→New, or on the New button) to open the data logging interface (Figure 11). This window is organized in four input sections: the first collects the beam dimensions, the second the set of boundary conditions, the third the properties of the cross-section of the beam and the fourth the geometric and material properties of the ballast mass.

In order to describe how to use the software, in the following we will describe the calculation of the first four eigenfrequencies and eigenmodes of the case study (Section 3.2) in Figure 2, considering a simply supported configuration.

First, we define the length a = 50 mm of the beam portion *OP*, the length $2b$ = 25 mm of the region *PQ* where the ballast massis introduced, and the length c = 25 mm of the beam portion *QR*. Second, we select the proper boundary condition (pinned) at each ends of the beam (*O*, *R*) among that available (fixed, pinned, free). Third, we introduce the elastic properties of the material and the geometric properties of the cross-section of the two beam portions (*OP*, *QR*). For the most common cross-sections, these data can be defined through a simple automatic calculation tools by clicking on the "Calc beam section properties" button. As an alternative, we can type the values in the proper field. For this configuration we have: E = 210000 MPa, ρ_{Beam} = 7850 kg/m^3, A = 10 mm^2, and I = 0.833 mm^4. Finally, we have to introduce the inertial properties of the ballast mass. Again a simple automatic calculation tool is available by clicking on the "Calc mass property" button. For this configuration we have to define the following values: m = 2.9438E-2 kg, J_{sz} = 2.2691E-6 kg m^2.

In addition, by clicking on the "Option" button we can personalize the analysis through the following three options. First, the number of eigenfrequencies to be calculated. Second, the convergence criteria in the solution of the transcendental equation (35). Third, the resolution of the diagrams containing the plot of the eigenmodes.

Clicking on the “Frequency Analysis” button the calculation starts. Once the solution process is concluded, the window of the results appears (Figure 12). On the left, we can see the diagrams of the normalized eigenmodes, while on the right a table summarizes the eigenfrequencies and eigenmodes. A scroll bar is available, in case the window is larger than the screen. By selecting “Export Results” it is possible to save the results of the analysis in a text file containing both the eigenfrequencies and the eigenmodes.

APPENDIX 2

In case of a inhomogeneous beam (Figure 13) having a constant width *r*, and constituted by *n* homogeneous layers with a thickness h_i , Young's modulus E_i and mass density ρ_i, the equivalent bending stiffness is can be written as [31]:

$$< EI_{z'} > = \sum_{i=1}^{n} E_i f \left[\frac{h_i^3}{12} + A_i \left(y_i - h_E \right)^2 \right] \tag{A1}$$

where h_E is the distance between the centre of elasticity of the inhomogeneous section and the longitudinal axis of the beam

Similarly, the equivalent mass density $\bar{\rho}$ of the composite material results in the following expression:

$$\bar{\rho} = \frac{\sum_{i=1}^{n} \rho_i A_i}{\sum_{i=1}^{n} A_i} \tag{A2}$$

Table and figure captions

Table 1 Sets of boundary conditions of the beam.

Table 2 Values of the parameters χ_1 , χ_2 , χ_3 , χ_4 , χ_5 , χ_6 as a function of the set of boundary conditions.

Table 3 Comparison between the RM model reduced to concentrated mass with or without inertia and analogous models from the literature.

Table 4 Geometric and inertial parameters of the case study (Figure 2) for the implementation of the RM model and of the two-dimensional FE model.

Table 5 Comparison between the results provided by the RM model and by the two-dimensional FE model for the first four eigenfrequencies of the case study (Figure 2).

Table 6 Comparison between the results provided by the three-dimensional FE model, by the RM model, by the concentrated mass model and by the concentrated mass and inertia model, for the first four eigenfrequencies of the case study (Figure 2).

Table 7 Young's modulus of the material of the ballast mass, corresponding bending stiffness both of the ballast massand of the beam and bending stiffness ratio φ.

Figure 1 Sketch of the beam structure with ballast mass (a) and simplification of the structure into two beam portions connected by a rigid link (b).

Figure 2 Sketch of the beam structure considered as case study in Section 3 (dimensions in mm)

Figure 3 First four eigenmodes for the fixed-free beam

Figure 4 First four eigenmodes for the fixed-fixed beam

Figure 5 First four eigenmodes for the fixed-pinned beam

Figure 6 First four eigenmodes for the pinned-pinned beam

Figure 7 First four eigenmodes for the free-free beam

Figure 8 Image of the mesh performed on the three-dimensional FE model

Figure 9 Plot of the percentage relative error in the prediction of the eigenfrequency as a function of the bending stiffness ratio, for a fixed-free beam

Figure 10 Plot of the percentage relative error in the prediction of the eigenfrequency as a function of the bending stiffness ratio, for a fixed-fixed beam

Figure 11 Data logging interface in the BFC software

Figure 12 Results window of the BFC software

Figure 13 Sketch of the cross-section of a composite beam

End conditions of beam $(O-R)$	Boundary Conditions at O	Boundary Conditions at R
Fixed – Free	$V_n(\xi=0)=0$ $V_n^{I}(\xi=0)=0$	$W_n^{II}(\eta=c)=0$ $W_n^{III}(\eta=c)=0$
Fixed – Fixed	$V_n(\xi=0)=0$ $V_n^{I}(\xi=0)=0$	$W_n(\eta=c)=0$ $W_n^{I}(\eta=c)=0$
Fixed – Pinned	$V_n(\xi=0)=0$ $V_n^{I}(\xi=0)=0$	$W_n(\eta=c)=0$ $W_n^{II}(\eta=c)=0$
Pinned – Pinned	$V_n(\xi=0)=0$ $V_n^{II}(\xi=0)=0$	$W_n(\eta=c)=0$ $W_n^{II}(\eta=c)=0$
Free – Free	$V_n^{II}(\xi=0)=0$ $V_n^{III}(\xi=0)=0$	$W_n^{II}(\eta=c)=0$ $W_n^{III}(\eta=c)=0$

Table 1

End conditions of beam $(O-R)$	χ_1	χ_2	χ_3	χ_4	χ_5	χ_6
Fixed – Free	1	0	-1	1	1	1
Fixed – Fixed	1	0	1	1	1	1
Fixed – Pinned	1	0	1	-1	$\tan(\beta_n c)$	$\tanh(\beta_n c)$
Pinned – Pinned	1	1	1	-1	$\tan(\beta_n c)$	$\tanh(\beta_n c)$
Free – Free	-1	0	-1	1	1	1

Table 2

Structure under examination	m/m_{beam}	$J/(m_{beam}*L^2)$	a/L	Reference	Mode	f_{adim} reference model	f_{adim} RM model
Fixed – free tip mass and inertia	0.6	0.4	1	[15]	1	1.12305	1.12305
					2	2.08695	2.08695
					3	4.98723	4.98723
					4	8.02840	8.02840
Fixed-fixed intermediate mass	0.6	0	0.75	[8]	1	4.25570	4.25570
					2	6.68237	6.68237
					3	10.19053	10.19053
					4	13.96990	13.96990
Fixed-pinned intermediate mass	0.6	0	0.75	[8]	1	3.31928	3.31928
					2	6.29730	6.29730
					3	9.93266	9.93266
					4	13.29452	13.29452
Pinned-pinned intermediate mass and inertia	0.6	0.4	0.75	[17]	1	1.94099	1.94099
					2	3.79828	3.79828
					3	5.57670	5.57670
					4	9.59831	9.59831
Free-free no mass	0	0	0	[21]	1	4.73005	4.73005
					2	7.85321	7.85321
					3	10.99561	10.99561
					4	14.13717	14.13717

Table 3

Geometric and material properties	RM model	CM model		2D FE model
		With Inertia	Without Inertia	
a (mm)	50	62.5	62.5	62.5
b (mm)	12.5	0	0	12.5
c (mm)	25	37.5	37.5	25
m (kg)	2.9438E-2	2.9438E-2	2.9438E-2	2.9438E-2
J_{sz} (kg m^2)	2.2691E-6	2.2691E-6	0	2.2691E-6

Table 4

Model Type		Eigenmode I		Eigenmode II		Eigenmode III		Eigenmode IV	
		Freq. (Hz)	Err %	Freq. (Hz)	Err %	Freq. (Hz)	Err %	Freq. (Hz)	Err %
Fixed - Free	**RM model**	**39.05**	**0.1**	**420.30**	**0.0**	**1587.40**	**0.0**	**2325.27**	**0.0**
	FE 2D	39.00		420.31		1587.50		2325.70	
Fixed - Fixed	**RM model**	**255.45**	**0.0**	**1019.92**	**0.0**	**2316.82**	**0.0**	**5991.26**	**0.0**
	FE 2D	255.35		1020.00		2317.00		5991.80	
Fixed - Pinned	**RM model**	**188.00**	**0.0**	**775.98**	**0.0**	**2301.83**	**0.0**	**5925.05**	**0.0**
	FE 2D	187.93		775.92		2301.80		5925.50	
Pinned - Pinned	**RM model**	**128.54**	**0.0**	**688.18**	**0.0**	**1679.59**	**0.0**	**4876.72**	**0.0**
	FE 2D	128.52		688.27		1679.70		4877.10	
Free - Free	**RM model**	**519.26**	**0.0**	**1583.91**	**0.0**	**2303.23**	**0.0**	**5992.77**	**0.0**
	FE 2D	519.24		1584.20		2303.60		5993.30	

Table 5

Model Type		Eigenmode I		Eigenmode II		Eigenmode III		Eigenmode IV	
		Freq. (Hz)	**Err %**	**Freq. (Hz)**	**Err %**	**Freq. (Hz)**	**Err %**	**Freq. (Hz)**	**Err %**
Fixed - Free	FE 3D	38.76		415.03		1549		2294.6	
	RM model	**39.05**	**0.7**	**420.3**	**1.3**	**1587.4**	**2.5**	**2325.27**	**1.3**
	CM model without inertia	38.38	-1.0	373.7	-10.0	1193.95	-22.9	2828.96	23.3
	CM model	37.66	-2.8	280.17	-32.5	774.89	-50.0	1430.31	-37.7
Fixed - Fixed	FE 3D	253.5		1005.1		2288.9		5905.8	
	RM model	**255.45**	**0.8**	**1019.92**	**1.5**	**2316.82**	**1.2**	**5991.26**	**1.4**
	CM model without inertia	177.59	-29.9	1159.84	15.4	2839.86	24.1	3810.3	-35.5
	CM model	175.77	-30.7	557.94	-44.5	1429.2	-37.6	3787.47	-35.9
Fixed -Pinned	FE 3D	185.53		763.24		2274.1		5813.2	
	RM model	**188**	**1.3**	**775.98**	**1.7**	**2301.83**	**1.2**	**5925.05**	**1.9**
	CM model without inertia	118.36	-36.2	1093.43	43.3	2140.14	-5.9	3515.94	-39.5
	CM model	118.36	-36.2	500.76	-34.4	1428.46	-37.2	2678.07	-53.9
Pinned - Pinned	FE 3D	126.36		675.51		1648.3		4785.4	
	RM model	**128.54**	**1.7**	**688.18**	**1.9**	**1679.59**	**1.9**	**4876.72**	**1.9**
	CM model without inertia	84.78	-32.9	765.42	13.3	1988.24	20.6	2950	-38.4
	CM model	84.42	-33.2	455.79	-32.5	1032.1	-37.4	2678.07	-44.0
Free - Free	FE 3D	515.08		1554.5		2269.6		5875.1	
	RM model	**519.26**	**0.8**	**1583.91**	**1.9**	**2303.23**	**1.5**	**5992.77**	**2.0**
	CM model without inertia	410.96	-20.2	1181.19	-24.0	2828.44	24.6	3791.07	-35.5
	CM model	344.88	-33.0	777.07	-50.0	1411.93	-37.8	3783.27	-35.6

Table 6

E_{mass} (GPa)	$<EI>_{mass}$ (Nm^2)	$<EI>_{beam}$ (Nm^2)	φ
632.2	1750	0.175	10000
210	591	0.175	3375
59.3	175	0.175	1000
28.25	87.6	0.175	500
4.95	17.5	0.175	100
2.375	8.76	0.175	50
0.4423	1.75	0.175	10

Table 7

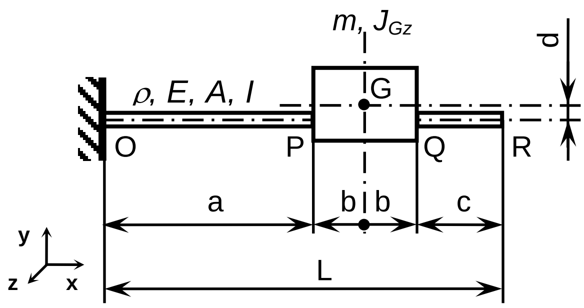
m, J_Gz
d
ρ, E, A, I
G
O
P
Q
R
a
b
b
c
L
y
z
x

(a)

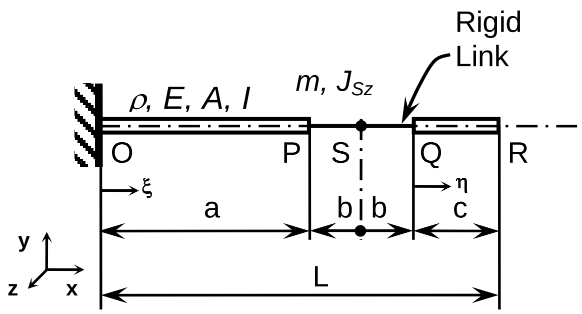
Rigid
Link
m, J_Sz
ρ, E, A, I
O
P
S
Q
R
ξ
η
a
b
b
c
L
y
z
x

(b)

Fig. 1

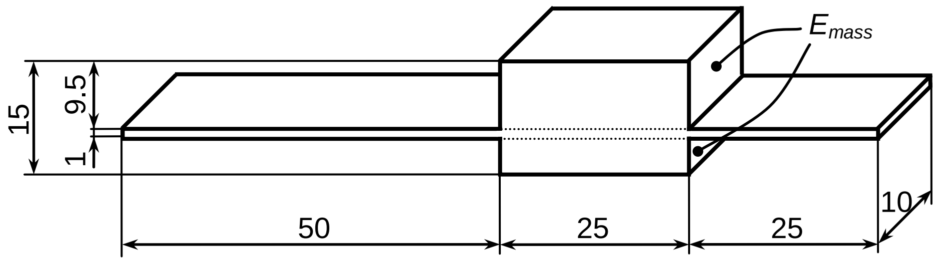

Fig. 2

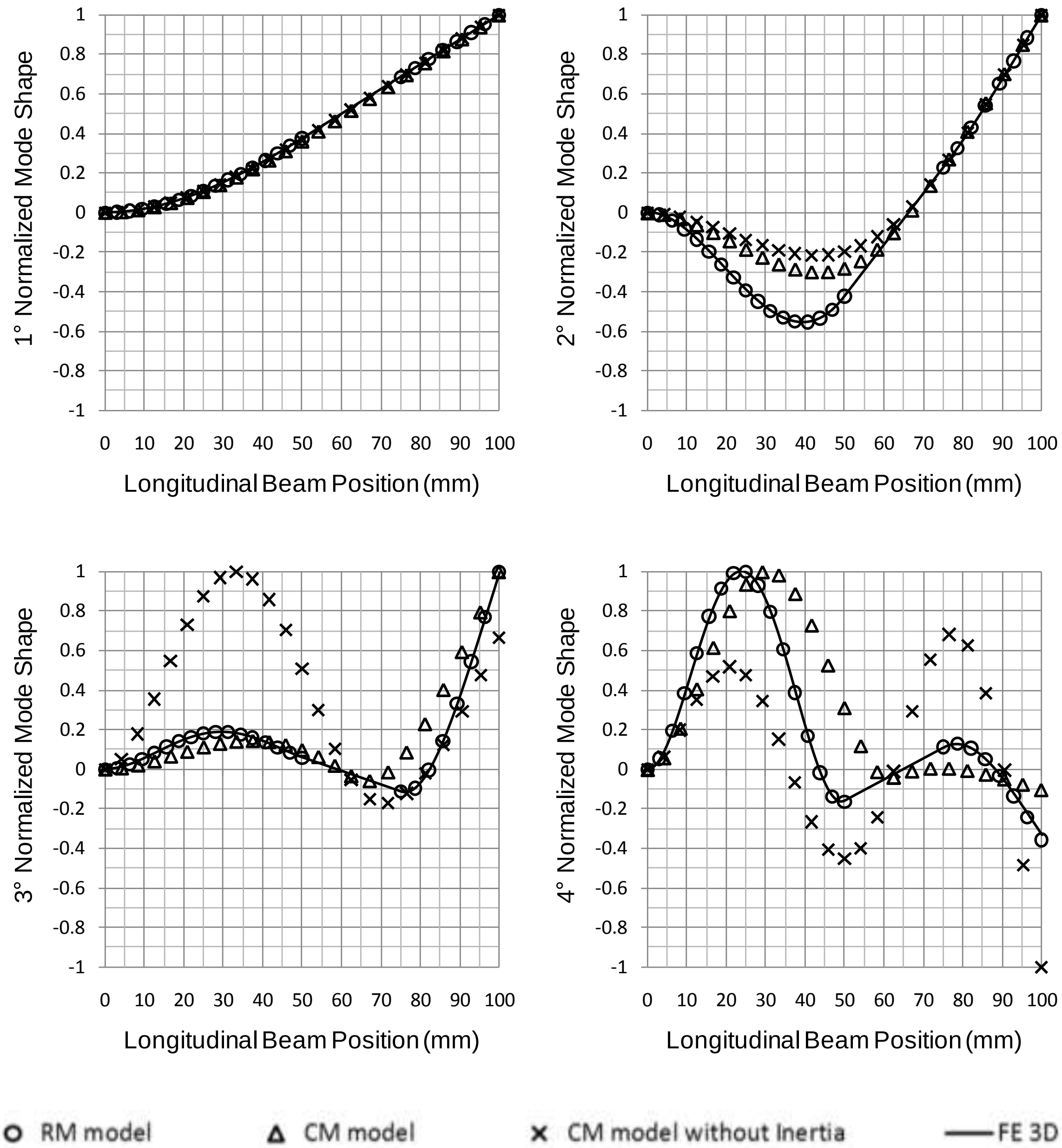
1° Normalized Mode Shape
2° Normalized Mode Shape
3° Normalized Mode Shape
4° Normalized Mode Shape
Longitudinal Beam Position (mm)
Longitudinal Beam Position (mm)
Longitudinal Beam Position (mm)
Longitudinal Beam Position (mm)
RM model
CM model
CM model without Inertia
FE 3D

Fig. 3

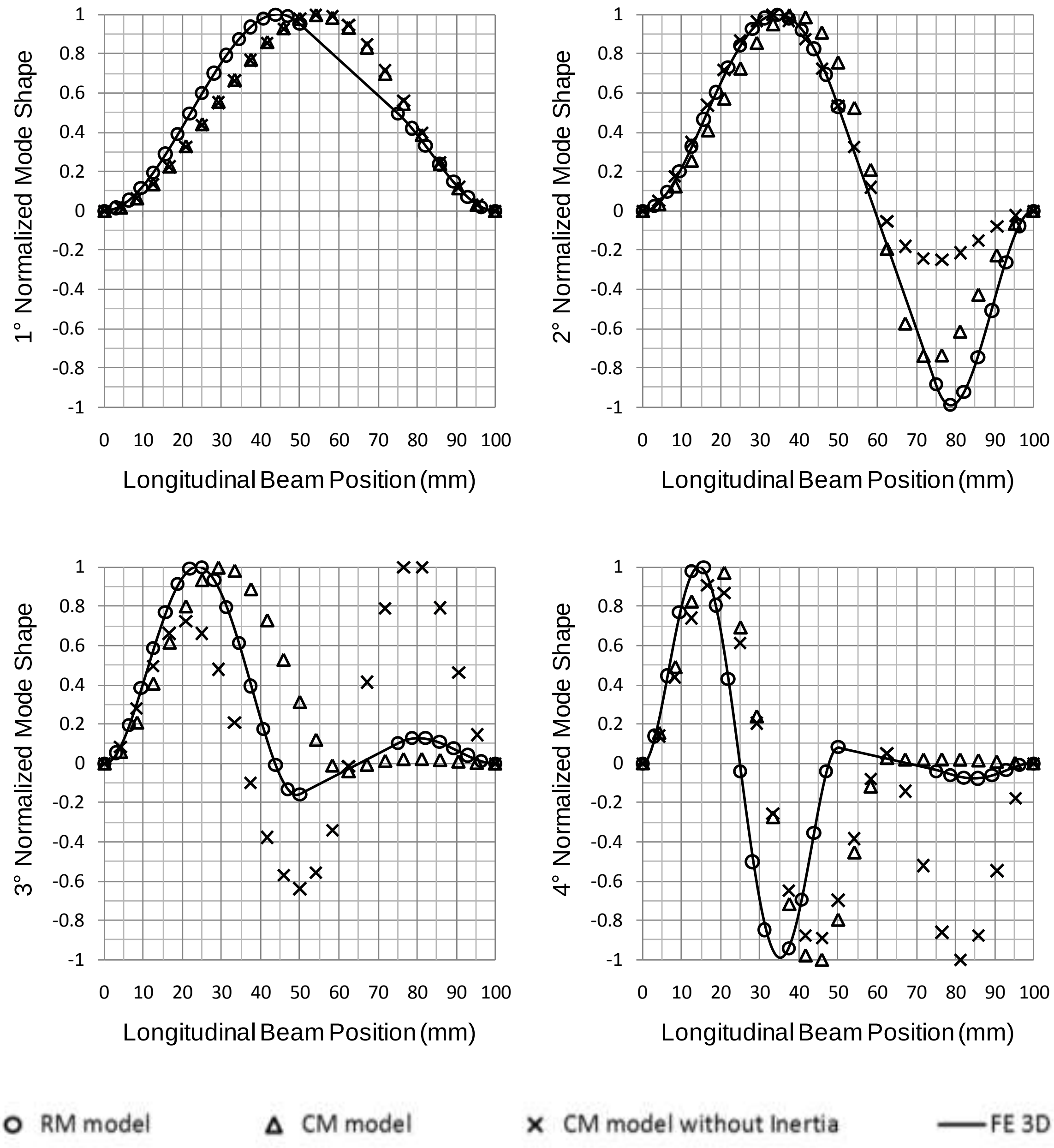
1° Normalized Mode Shape
2° Normalized Mode Shape
3° Normalized Mode Shape
4° Normalized Mode Shape
Longitudinal Beam Position (mm)
RM model
CM model
CM model without Inertia
FE 3D

Fig. 4

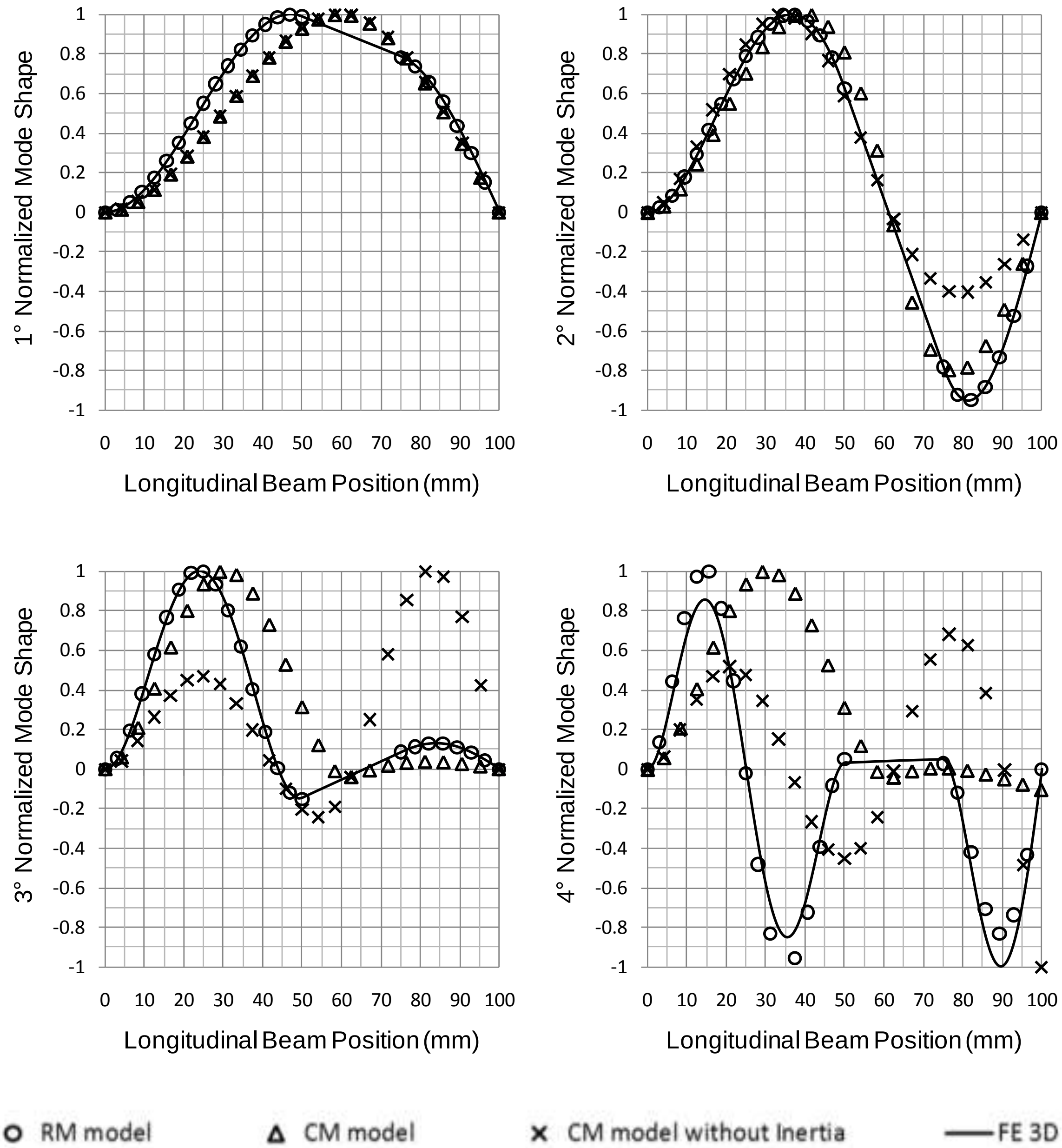
1° Normalized Mode Shape
2° Normalized Mode Shape
3° Normalized Mode Shape
4° Normalized Mode Shape
Longitudinal Beam Position (mm)
RM model
CM model
CM model without Inertia
FE 3D

Fig. 5

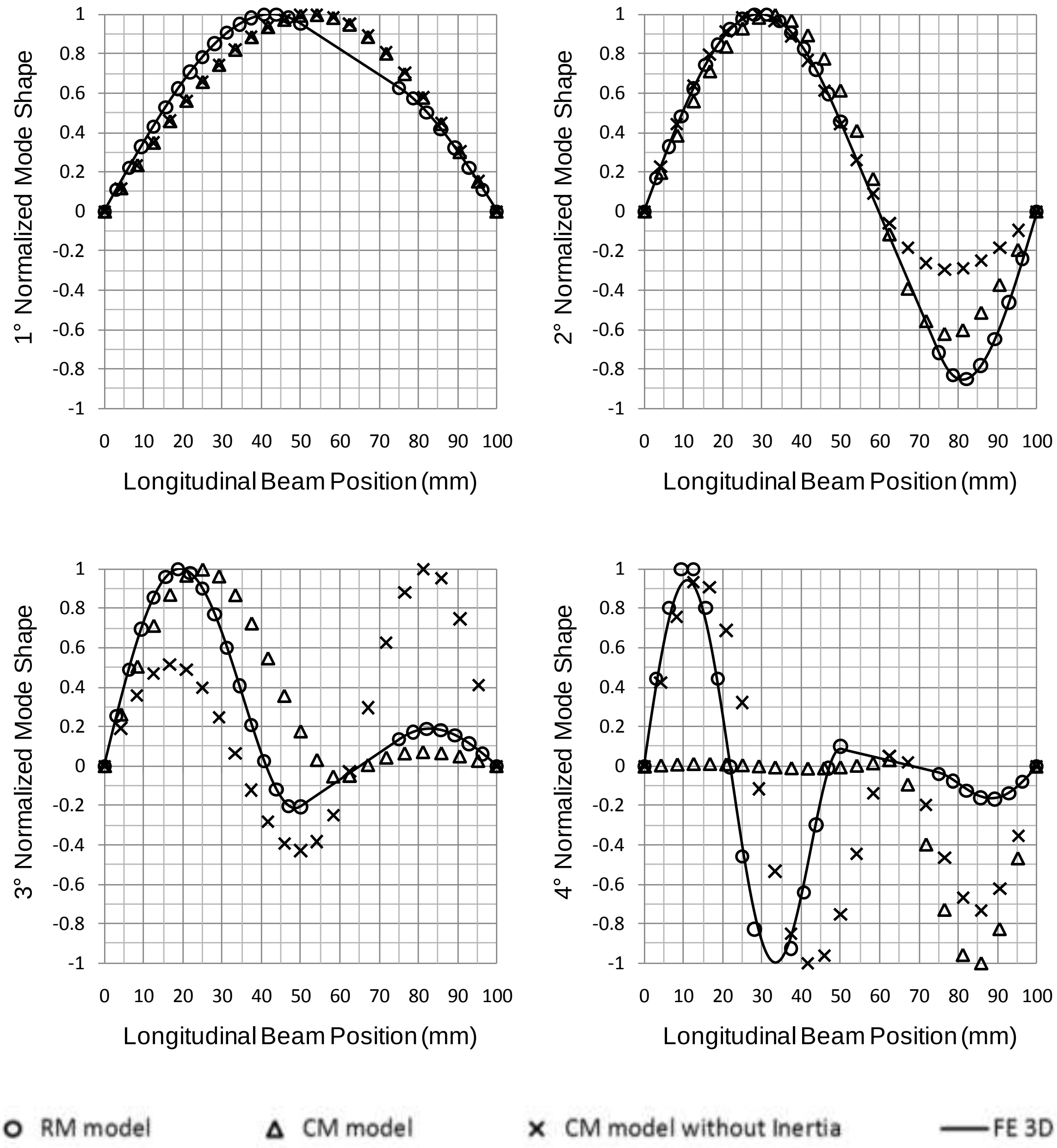
1° Normalized Mode Shape
2° Normalized Mode Shape
3° Normalized Mode Shape
4° Normalized Mode Shape
Longitudinal Beam Position (mm)
RM model
CM model
CM model without Inertia
FE 3D

Fig. 6

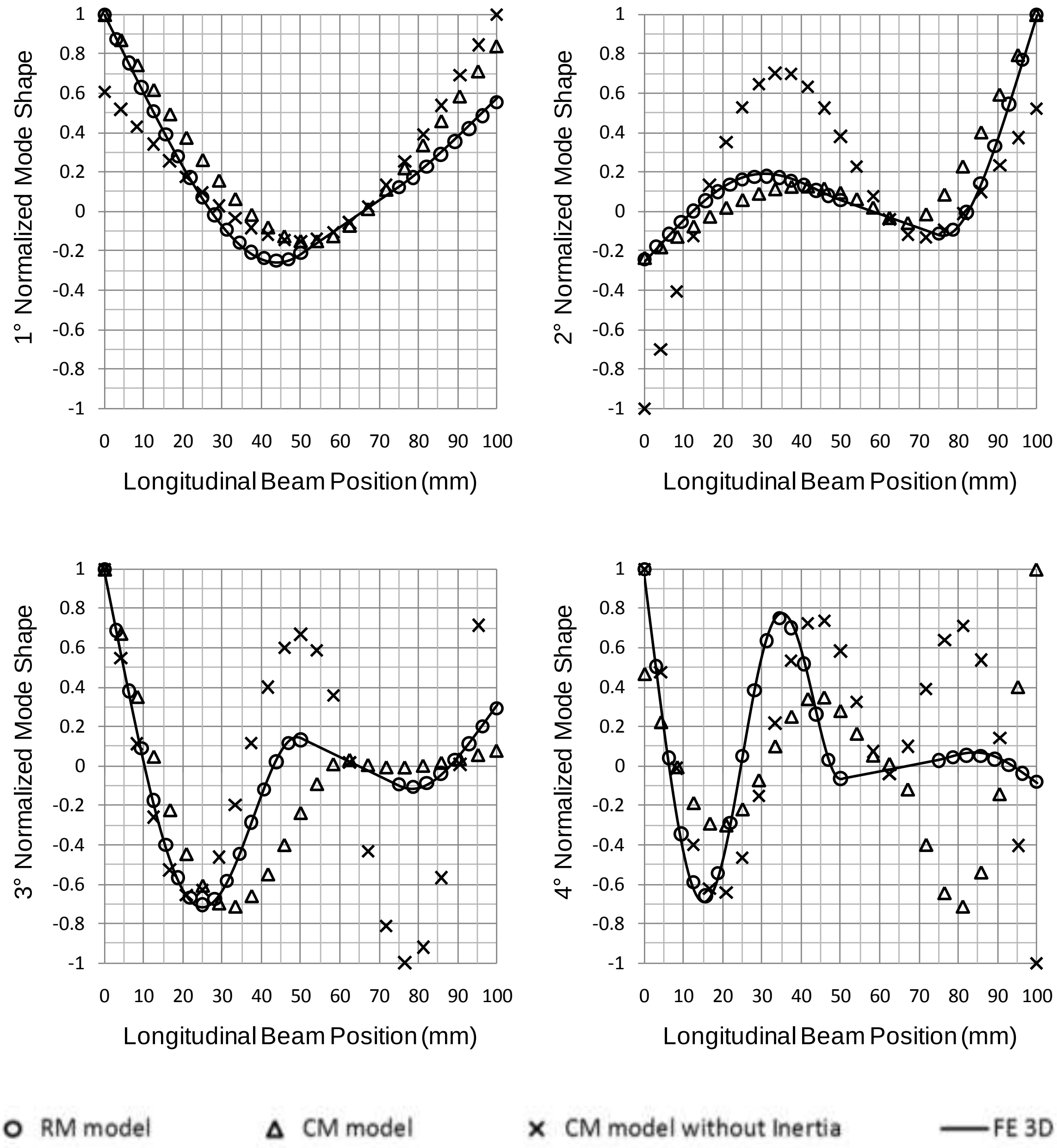
1° Normalized Mode Shape
2° Normalized Mode Shape
3° Normalized Mode Shape
4° Normalized Mode Shape
Longitudinal Beam Position (mm)
RM model
CM model
CM model without Inertia
FE 3D

Fig. 7

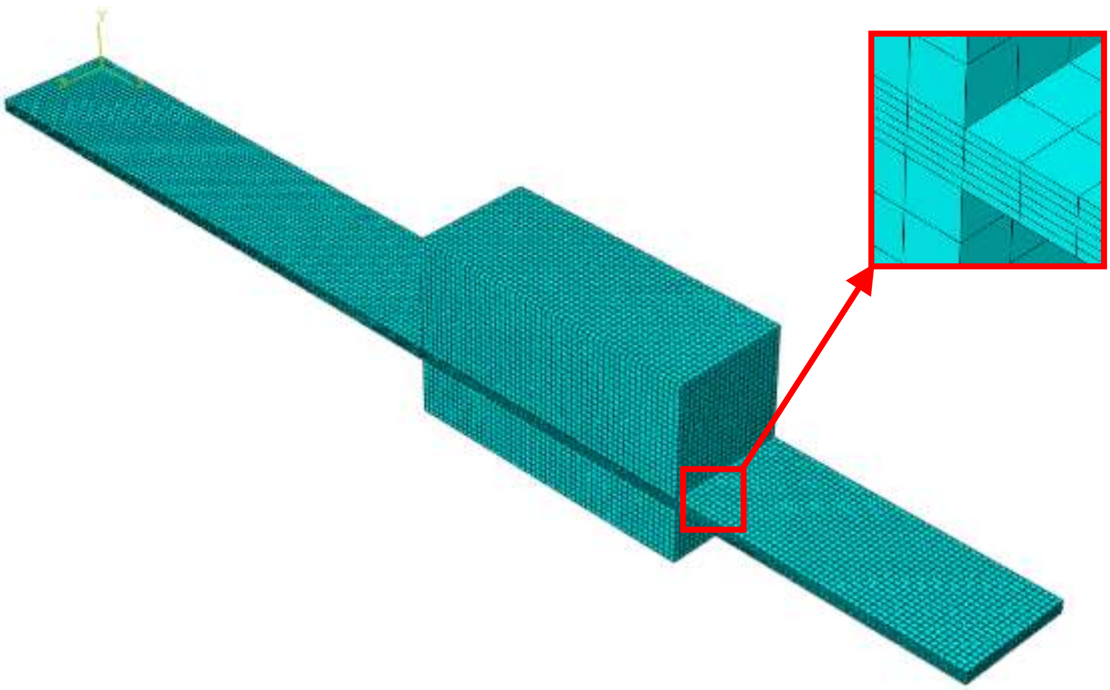

Fig. 8

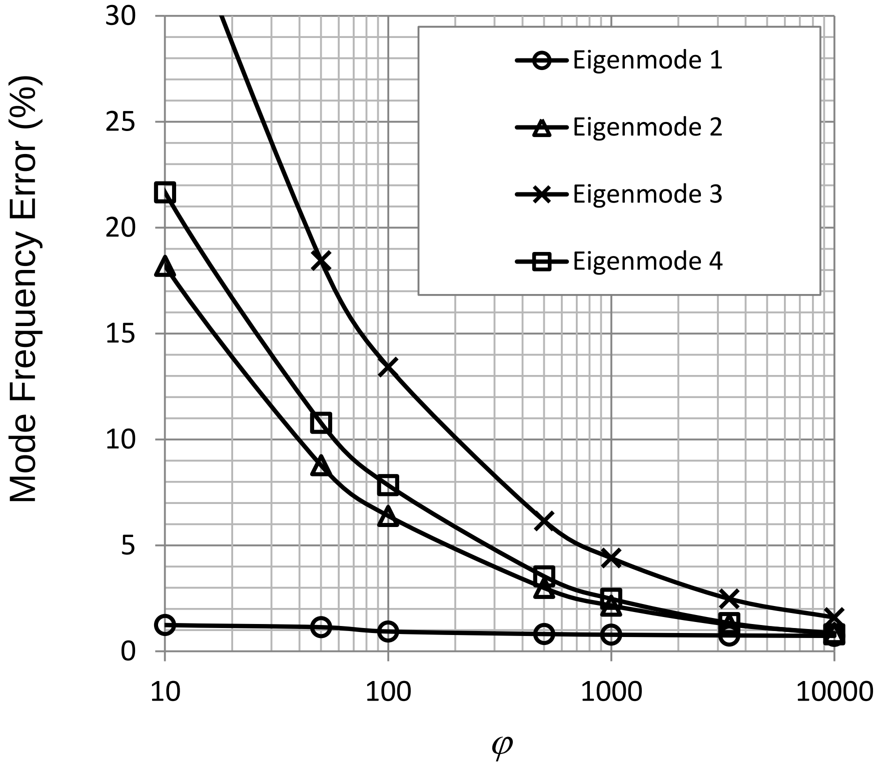
Mode Frequency Error (%)
30
25
20
15
10
5
0
10
100
1000
10000
φ
Eigenmode 1
Eigenmode 2
Eigenmode 3
Eigenmode 4

Fig. 9

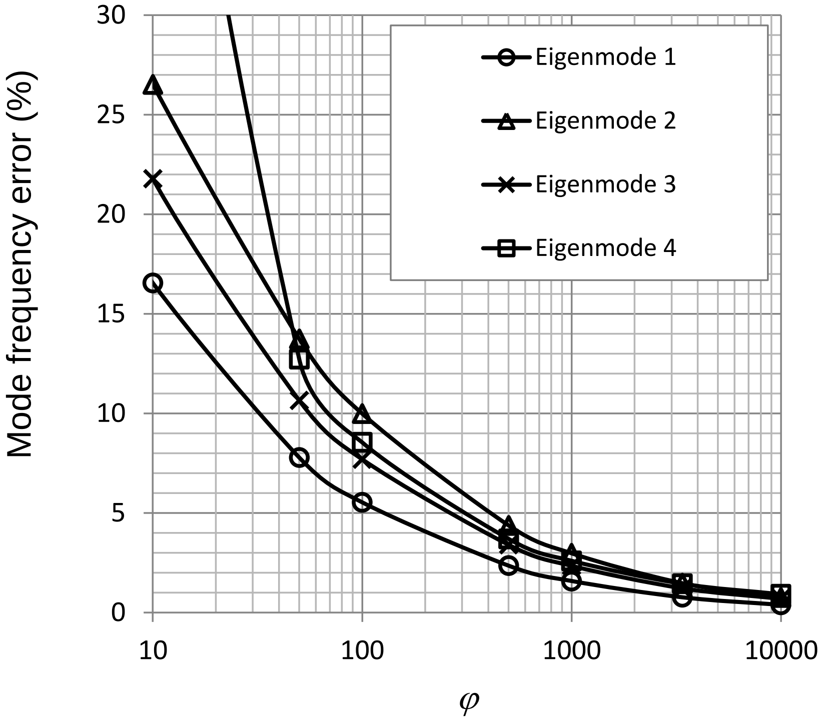
Mode frequency error (%)
30
25
20
15
10
5
0
10
100
1000
10000
φ
Eigenmode 1
Eigenmode 2
Eigenmode 3
Eigenmode 4

Fig. 10

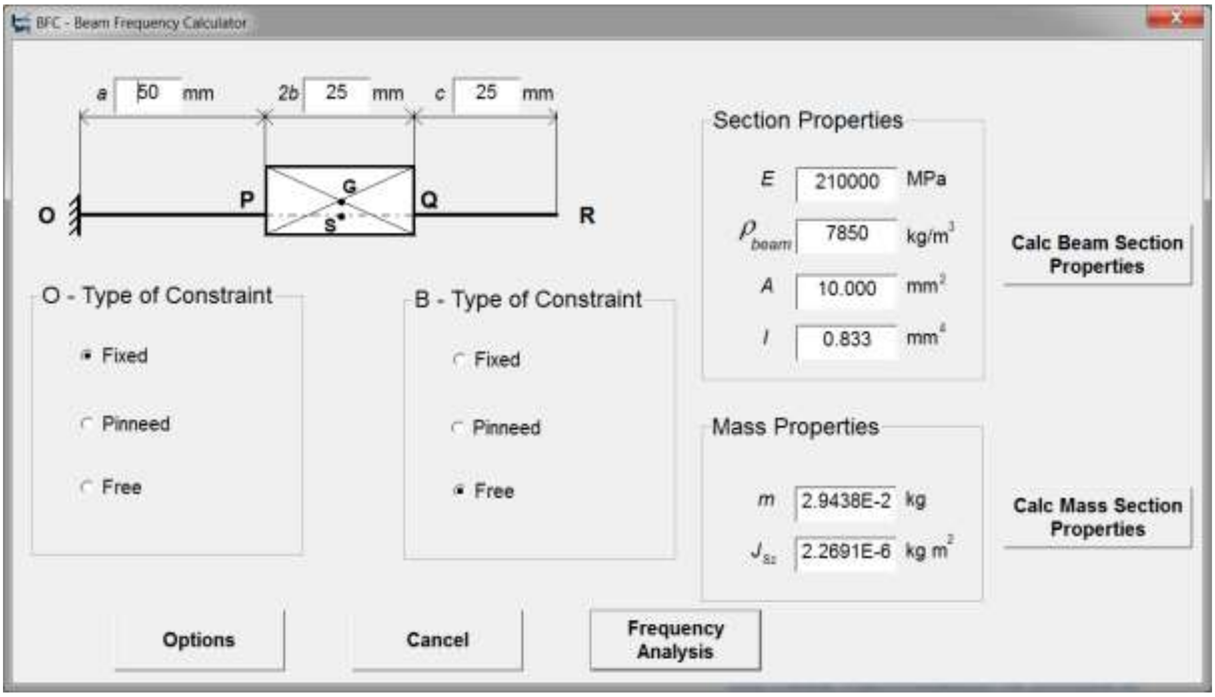
BFC - Beam Frequency Calculator
a
50
mm
2b
25
mm
c
25
mm
O
P
G
S
Q
R
Section Properties
E
210000
MPa
ρ beam
7850
kg/m3
A
10.000
mm2
I
0.833
mm4
Calc Beam Section Properties
O - Type of Constraint
Fixed
Pinneed
Free
B - Type of Constraint
Fixed
Pinneed
Free
Mass Properties
m
2.9438E-2
kg
J Sz
2.2691E-6
kg m2
Calc Mass Section Properties
Options
Cancel
Frequency Analysis

Fig. 11

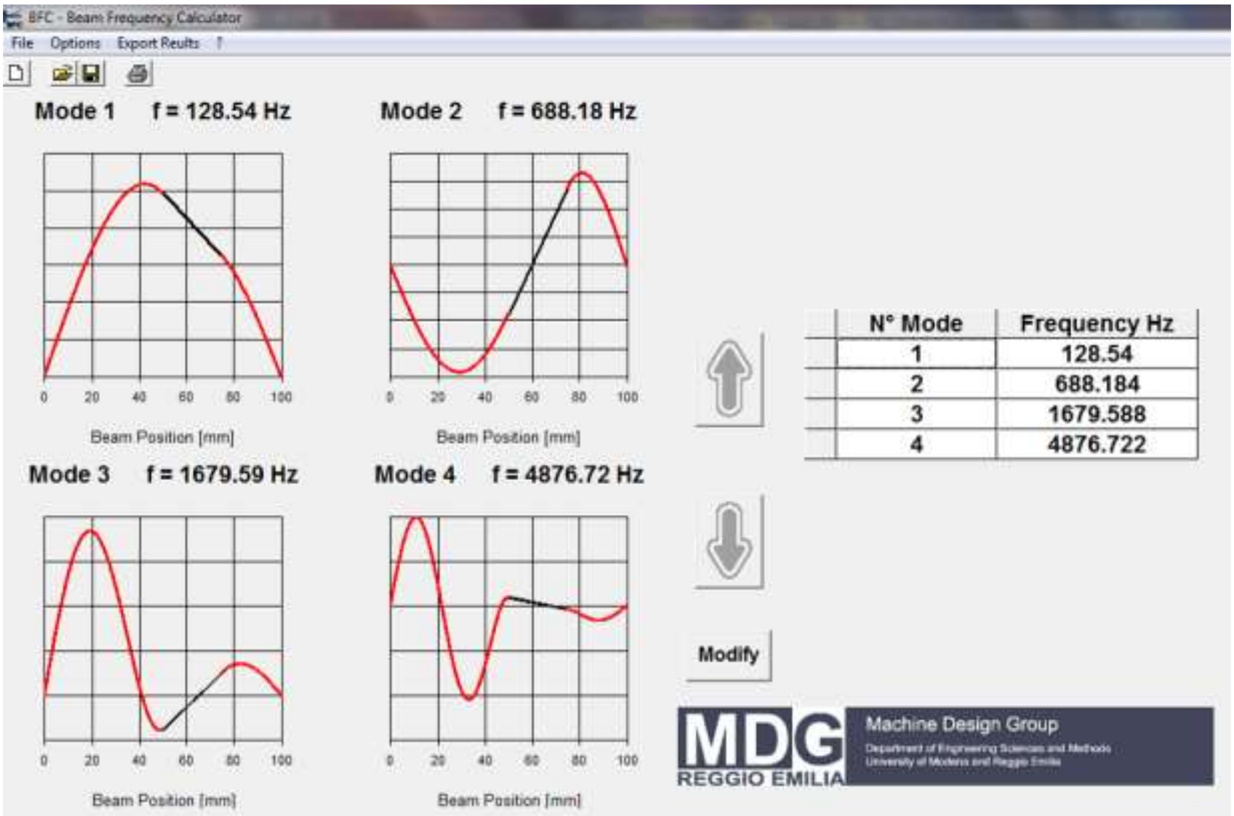
BFC - Beam Frequency Calculator
File Options Export Reults ?
Mode 1 f = 128.54 Hz
Mode 2 f = 688.18 Hz
Mode 3 f = 1679.59 Hz
Mode 4 f = 4876.72 Hz
0 20 40 60 80 100
Beam Position [mm]
N° Mode
Frequency Hz
1 128.54
2 688.184
3 1679.588
4 4876.722
Modify
MDG
REGGIO EMILIA
Machine Design Group

Fig. 12

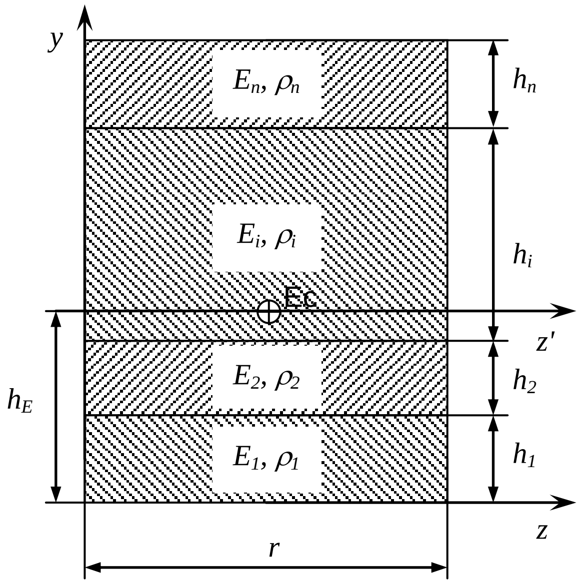

Fig. 13